


**Please cite the Published Version**

Garnayak, Subrat, Elbaz, Ayman M, Kuti, Olawole , Dash, Sukanta Kumar, Roberts, William L and Reddy, V Mahendra (2022) Auto-ignition and numerical analysis on high-pressure combustion of premixed methane-air mixtures in highly preheated and diluted environment. Combustion Science and Technology, 194 (15). pp. 3132-3154. ISSN 0010-2202

**DOI:** <https://doi.org/10.1080/00102202.2021.1909579>

**Publisher:** Taylor & Francis

**Version:** Accepted Version

**Downloaded from:** <https://e-space.mmu.ac.uk/629711/>

**Usage rights:**  [Creative Commons: Attribution-Noncommercial 4.0](https://creativecommons.org/licenses/by-nc/4.0/)

**Additional Information:** This is an Accepted Manuscript of an article published by Taylor & Francis in Combustion Science and Technology on 19th April 2021, available at: <http://www.tandfonline.com/10.1080/00102202.2021.1909579>. It is deposited under the terms of the Creative Commons Attribution-NonCommercial License (<http://creativecommons.org/licenses/by-nc/4.0/>), which permits non-commercial re-use, distribution, and reproduction in any medium, provided the original work is properly cited.

**Data Access Statement:** Supplemental data for this article can be accessed in publisher's website

**Enquiries:**

If you have questions about this document, contact [openresearch@mmu.ac.uk](mailto:openresearch@mmu.ac.uk). Please include the URL of the record in e-space. If you believe that your, or a third party's rights have been compromised through this document please see our Take Down policy (available from <https://www.mmu.ac.uk/library/using-the-library/policies-and-guidelines>)

# **Auto-Ignition and Numerical Analysis on High-Pressure Combustion of Premixed Methane-Air mixtures in Highly Preheated and Diluted Environment**

**Subrat Garnayak<sup>1</sup>, Ayman M Elbaz<sup>3</sup>, Olawole Kuti<sup>2</sup>, Sukanta Kumar Dash<sup>4</sup>, William L  
Roberts<sup>3\*</sup>, V. Mahendra Reddy<sup>4\*</sup>**

<sup>1</sup>School of Energy Science and Engineering, IIT Kharagpur, India-721302

<sup>2</sup>Department of Engineering, the Manchester Metropolitan University, Chester Street, M1 5GD,  
Manchester, United Kingdom

<sup>3</sup>Clean Combustion Research Center, King Abdullah University of Science and Technology  
(KAUST), Thuwal 23955, Saudi Arabia

<sup>4</sup>Department of Mechanical Engineering, IIT Kharagpur, India-721302

---

Corresponding author: [mahendra@iitkgp.ac.in](mailto:mahendra@iitkgp.ac.in); [William.roberts@kaust.edu.sa](mailto:William.roberts@kaust.edu.sa)

**Abstract**

The present work investigates both the autoignition and the combustion characteristics on highly preheated and diluted combustion of laminar premixed stoichiometric  $\text{CH}_4/\text{O}_2/\text{N}_2$  mixture in a cylindrical combustor operating at elevated pressure. The analysis has been carried out for a range of operating parameters such as reactant preheat temperature of 1100-1500 K, combustor pressure of 1-10 atm, and highly diluted mixture, which is achieved by decreasing the oxygen content in the oxidizer from 21 to 3% in volume basis. The simulations have been carried out using the laminar premixed adiabatic PFR (plug flow reactor) model of Ansys Chemkin Pro. Two-dimensional pictorial representation is carried out using finite volume-based CFD code Ansys Fluent 19.2. Finite-rate chemistry with detailed chemical mechanism GRI Mech 3.0 is used for combustion analysis. The results show that OH and HCO mole fractions are decreased with increased combustor pressure and  $\text{N}_2$  dilution (or decreased  $\text{O}_2$  content) while it increases with the reactant's temperature. Also, it has been found that by reducing the oxygen content in the mixture, the flame gets stabilized far away from the combustor inlet. In contrast, an increase in combustor pressure and reactant temperature stabilize the flame towards the combustor inlet. The flame stabilization characteristics at different locations of the combustor are explained in terms of ignition delay time, which is calculated using the closed homogenous reactor (CHR) model available in the Ansys Chemkin Pro package. The flame peak temperature decreases with an increase in  $\text{N}_2$  dilution and increases with increasing the reactant temperature. Moreover, the peak temperature varies marginally with increasing the combustor pressure. Finally, a regime diagram is prepared to show the various combustion mode such as HiTAC, MILD combustion, and No ignition region as a function of  $\text{O}_2$  content and reactant temperature for different operating pressure. The CO and NO emission are reduced with an increase in pressure in the MILD combustion region.

**Keywords:** Highly preheated and diluted combustion; high pressure; CFD; Ignition delay; MILD combustion

## **1. Introduction**

Highly preheated and diluted combustion or high-temperature air combustion (HiTAC) is a novel technology developed for energy savings, flame stability enhancement, and reduction of significant pollutant emissions like NO<sub>x</sub> and CO (Katsuki and Hasegawa, 1998; Rafidi et al., 2008; Gupta, 2003). This technology is based on preheating and diluting the fresh gases with the flue gases that result in more uniform temperature distribution and lower NO<sub>x</sub> emission than the combustor operating under conventional mode. It has been implemented in many industrial and experimental applications, and also developed and reported with a different name such as Flameless oxidation (FLOX)( Wüning and Wüning, 1997), Colorless distributed combustion (CDC)( Arghode and Gupta, 2011), MILD combustion (Cavaliere and De Joannon, 2004). While these technologies have commonalities and work on a similar concept as HiTAC combustion, they are not the same. Flameless combustion is related to the fact that there is no visible flame appearance, mainly due to the high exhaust gas recirculation rates and distributed combustion with the low-temperature gradient (Wüning and Wüning, 1997; Reddy et al., 2015).

Similarly, the CDC is based on higher combustion intensities and lower residence time than HiTAC combustion (Arghode and Gupta, 2011). On the other hand, MILD combustion is a subset of HiTAC combustion, in which the inlet reactant temperature should be above the self-ignition temperature, and the maximum temperature increase inside the combustor should be less than the mixture self-ignition temperature (Cavaliere and De Joannon, 2004). In HiTAC, the combustion air is preheated above the auto-ignition temperature and can operate in both MILD and non-MILD combustion modes (Katsuki and Hasegawa, 1998). Experimental and

computational analyses have been conducted to understand this technique's reaction, flow, and emission characteristics (Khalil and Gupta, 2018; Chen et al., 2017; Christo and Dally, 2005). The effect of phase and heating value of fuels on achieving distributed combustion is deeply investigated (Mao et al., 2017; Reddy et al., 2014). However, most of the work has been reported on highly preheated and diluted combustion operating at ambient pressure, and less work is reported at high pressure. In the high-pressure MILD combustion, the increased pressure and the preheated reactants shorten the ignition delay to multiple orders than the distributed combustion at ambient pressure. Hence, distributed or MILD combustion at high pressure is still ambiguous. As suggested by (Sabia et al., 2015; Sabia et al., 2015; Sabia et al., 2014; De Joannon et al., 2002), the leading parameters affecting the occurrence of MILD combustion are inlet temperature of the reactants, operating pressure of the combustor, dilution level of the oxidizer and C/O ratio of the local fuel-air mixture. These parameters critically influence the autoignition delay time. The ignition delay time ( $\tau_{ign}$ ) is inversely proportional to both operating pressure ( $P_{comb}$ ) and inlet temperature ( $T_{reactants}$ ) of the reactants ( $\tau_{ign} \propto \frac{1}{P_{comb}}$ ;  $\tau_{ign} \propto \frac{1}{T_{reactants}}$ ). However, the dilution level ( $R_{dil}$ ) of the reactants has a direct relation with the auto-ignition delay time ( $\tau_{ign}$ ), i.e. ( $\tau_{ign} \propto R_{dil}$ ). Sidey et al. (2014) have identified MILD combustion regime boundary while investigating the constant pressure auto-ignition and freely propagating premixed flame of cold methane-air mixtures diluted with hot products. Recently, Shao et al. (2019) measured ignition delay times for methane and hydrogen fuels too diluted with CO<sub>2</sub> in a high-pressure shock tube. The measurements were carried out for a pressure range of 27-286 atm and a mixture temperature range of 1045-1578 K. Their study shows that the auto-ignition delay time is a vital function of both operating pressure and temperature. Hu et al. (2015) proposed a fitting correlation (Eq. (1)) of ignition delay times ( $\tau$ ) as a function of equivalence ratio ( $\phi$ ), pressure ( $p$ ), and temperature ( $T$ )

for methane-air mixtures through regression analysis with a co-efficient of determination  $R^2=0.983$ .

$$\tau = 1.09 \times 10^{-3} p^{-0.68} \phi^{-0.04} \exp\left(\frac{40.98 \pm 0.51 \text{ kcal.mole}^{-1}}{RT}\right) \quad (1)$$

Where  $\tau$  is the ignition delay time in  $\mu\text{s}$ ,  $p$  is pressure in atm,  $R = 1.983 \times 10^{-6} \text{ kcal/mol.K}$  is the universal gas constant, and  $T$  is the temperature of the reactant in Kelvin. This correlation is applicable for the pressure range of 1-10 atm, a temperature range of 1300-1900 K, and an equivalence ratio of 0.5-2.0. De Toni et al. (2017) measured ignition delay times for Jet A1 fuel using a rapid compression machine (RCM) and high-pressure shock tube for the pressure range from 7-30 atm, a temperature range of 670-1200 K, and fuel/air equivalence ratio of 0.3 to 1.3. They have developed a correlation (Eq. (2)) of ignition delay times for Jet A1 fuel through multiple linear regression analysis.

$$\tau/\mu\text{s} = 10^{2.06 \pm 0.22} \exp\left(\frac{14510 \pm 490}{T/K}\right) \times (p/\text{bar})^{-0.89 \pm 0.12} (\phi)^{-0.79 \pm 0.06} \quad (2)$$

The developed correlation is determined for the pressure ranging from 7-30 atm, temperature ranging from 925 -1195 K for the equivalence ratio ( $\phi$ ) from 0.3 and 1.0.

Few research groups studied distributed combustion in the highly preheated and diluted environment at elevated pressure. Khalil and Gupta (2011) have used CDC in a cylindrical gas turbine combustor incorporating tangential air inlet and axial exhaust gas outlet. They have conducted experiments on both premixed and non-premixed combustion regimes operating at 2.0 atm pressure and preheated inlet air using methane gas as a fuel. Luckcrath et al. (2008) achieved MILD combustion at 20 atm pressure for natural gas with and without  $\text{H}_2$  admixtures under different lean premixed conditions. Ye et al. (2015) experimentally achieved MILD combustion at a pressure of 5.0 atm in a reverse flow combustor by using pre-evaporated liquid fuels of ethanol,

acetone, and n-heptane. Kruse et al. (2015) investigated MILD combustion in a reverse flow configuration type combustor using methane as fuel in partially premixed mode operating at an atmospheric and elevated pressure of 2.5 and 5.0 atm. Tu et al. (2020) numerically investigated MILD combustion at high pressure up to 8 atm in a reverse flow configuration type non-premixed combustor using methane as a fuel. Their analysis suggests that MILD combustion at elevated pressure can be achieved by enhancing internal flue gas recirculation by decreasing the nozzle diameter.

From the above literature, it has been found that very little literature is available on high-pressure MILD combustion since the MILD combustion at very high pressure is a challenging task. To achieve the MILD combustion at high pressure, the combustion products need to be highly diluted. Consequently, the present study aims to accomplish the highly preheated and diluted combustion of laminar premixed  $\text{CH}_4/\text{O}_2/\text{N}_2$  mixture at high pressure (up to 10 atm.). Autoignition characteristics and numerical analyses are carried out to gain a detailed understanding of highly preheated and diluted combustion operating at high pressure. The ambient pressure varies from 1 to 10 atm, the temperature of the reactants is varied from 1100 to 1500 K, and the dilution of the reactants is varied from 21 to 3 %  $\text{O}_2$  (in volume) levels. The equivalence ratio of the mixture is maintained constant throughout our studies at  $\Phi = 1$ . The ignition delay as a function of combustor pressure, reactant temperature, and dilution is estimated by using Ansys CHEMKIN PRO considering the homogeneous reactor model. Simulation is conducted using the laminar plug flow reactor model (PFR) of the Ansys Chemkin Pro package. Two-dimensional pictorial representation of premixed methane ( $\text{CH}_4$ ) – diluted oxidizer is analyzed using the finite volume-based CFD code Ansys Fluent 19.2. Finite-rate chemistry with the widely used detailed chemical mechanism GRI MECH 3.0 (Smith et al., 2019) is implemented for the combustion analysis. The effects of the

ambient pressure, reactant temperature, and dilution on the flame and reaction distribution are investigated. Finally, a regime diagram is prepared to show the various combustion mode such as HiTAC, MILD combustion, and No ignition region as a function of  $O_2$  content and reactant temperature for different operating pressure.

## **2. Numerical modeling**

### **2.1. Ignition delay time**

The ignition delay of the  $CH_4/O_2/N_2$  mixture has been evaluated by considering the closed homogenous reactor model of the CHEMKIN PRO package. It has been assumed that the unburned gas mixture is in a closed adiabatic system during the computations. The transient, spatially homogeneous form of the conservation equations for mass, energy, and species are solved under such conditions. There are various methods available to estimate ignition delay times in computational as well as experimental combustion work. For instance, it is often defined as the time at which (i) the concentration of certain species reaches the maximum value, or (ii) the rate of increase in temperature reaches a particular user-defined value, or (iii) the output of the luminous radiation from the system is first noticed. In the present work, the ignition delay time is calculated using detailed chemical mechanism GRI Mech 3.0 (Smith et al., 2019) based on the approach related to the maximum of the OH species concentration. Surface chemistry is not included in the present computation. The GRI Mech 3.0 chemical mechanism contains 53 species and 325 chemical reactions. This mechanism was optimized and validated for methane and natural gas over a wide range of operating parameters, a temperature range of 1000-2500 K, pressure range from 10 Torr to 10 atm, based on flame speed measurement and shock tube experiment. Recently, (Tu et al., 2020) have validated GRI Mech 3.0 with experimentally measured data of ignition delay



time and laminar flame speed from 1 to 10 atm and implemented this mechanism for their CFD investigation on high-pressure MILD combustion. The performance of GRI Mech 3.0 in the highly diluted condition is good and also adopted by many combustion researchers in the area of MILD combustion studies even if at low  $O_2$  ( $Y_{O_2}=3\%$  in the oxidizer) content (Dally et al., 2005, Mardani and Mahalegi, 2019). Here, we have presented the prediction capability GRI Mech 3.0 by comparing the experimentally measured ignition delay times of  $CH_4/O_2/N_2$  mixtures at different  $N_2$  diluted conditions (Zeng et al., 2015) with two operating pressure of 1 and 10 atm, as shown in Fig.1. The GRI Mech 3.0 offers good agreement with experimental data in diluted conditions at atmospheric and elevated pressure of 10 atm. Hence, the GRI mech 3.0 chemical mechanism is considered in our present numerical analysis.

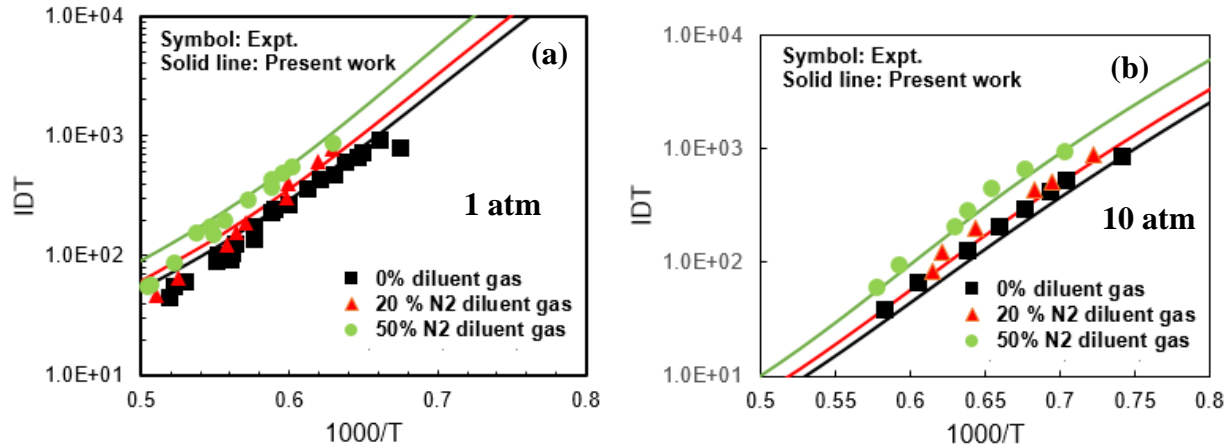


**Figure 1.** Validation of Chemkin results with measured experimental data of ignition delays of methane/ air mixtures diluted by  $N_2$ .

## 2.2. Laminar PFR model

In the present study, numerical simulation of a steady, one-dimensional, constant pressure laminar premixed flame in highly preheated and diluted conditions was conducted using the adiabatic plug flow reactor model (PFR) module Ansys Chemkin Pro and GRI 3.0 chemistry. The

plug flow reactor model is computationally efficient since it solves the first-order ordinary differential equations (ODE's) of continuity, momentum, energy, and species without requiring the transport properties. The fundamental assumption of a plug flow reactor model is that the fluid is perfectly mixed in the radial direction while there is no mixing in the axial direction. The present work considers the domain of length 1.4 m and diameter of 0.01m in which the combustion of laminar premixed CH<sub>4</sub>/O<sub>2</sub>/N<sub>2</sub> mixture in a diluted and at high-pressure condition is analyzed. The present reactor's dimension is taken from the experimental tubular reactor used by Sabia et al. (2013). A stoichiometric premixed mixture ( $\phi=1$ ) of CH<sub>4</sub> and oxidizer (O<sub>2</sub> and N<sub>2</sub>) is considered with different O<sub>2</sub> dilution levels. Reactants are supplied at the inlet at different reactant temperatures ranging from 1100 to 1500K. The percentage of O<sub>2</sub> in the air is varied from 21 to 3%. The pressure of the reactor is varied from 1 to 10 atm. The calculated jet Reynolds number of the mixture for all covered cases is  $\approx 1750$ . The effects of all these parameters (%O<sub>2</sub>, combustor pressure, inlet temperature) on achieving distributed combustion are investigated in the present work. At the combustor's inlet, mass flow inlet boundary condition is applied with a constant mixture mass flow rate of 0.00061 kg/s for all the cases considered in the present work. The mixture's mass flow rate is calculated by considering the inlet velocity of 30 m/s as the base case for the reactant temperature of 1300 K and at a pressure of 1 atm with a 21% O<sub>2</sub> level. The operating conditions considered in the present work, as well as corresponding flow velocity under stoichiometric conditions for all cases, are supplied in Table S1 of the supplementary material. Similarly, the mole fraction of the mixture species (CH<sub>4</sub>, O<sub>2</sub>, and N<sub>2</sub>) provided at the inlet with different dilution levels for  $\phi=1$  are listed in Table 1.

**Table 1:** Mixture composition (in mole fraction) for  $\phi=1$ 

<b>O<sub>2</sub> in the air (%)</b>	<b>N<sub>2</sub> in the air (%)</b>	<b>X<sub>CH<sub>4</sub></sub></b>	<b>X<sub>O<sub>2</sub></sub></b>	<b>X<sub>N<sub>2</sub></sub></b>
21	79	0.095	0.19	0.715
17	83	0.078	0.156	0.766
13	87	0.061	0.122	0.817
9	91	0.043	0.086	0.871
5	95	0.02439	0.04878	0.92683
3	97	0.01477	0.02955	0.95568

### 2.3. CFD Modelling

In the present work, laminar premixed combustion of CH<sub>4</sub>/O<sub>2</sub>/N<sub>2</sub> in a cylindrical combustor (tube) of 0.01m in diameter (D) and 1.4 m in length (L) is numerically analyzed. The same operating conditions, such as reactant temperature, pressure, and dilution level mentioned in the PFR model, are considered in the CFD study. The computational domain imposed with different boundary conditions is shown in Fig. 2. The wall of the combustor is set as adiabatic. At the inlet of the combustor, mass flow inlet boundary condition is applied with a constant mixture mass flow rate of 0.00061 kg/s for all the cases considered in the present work. Similarly, the mole fraction of the mixture species (CH<sub>4</sub>, O<sub>2</sub>, and N<sub>2</sub>) supplied at the inlet with different dilution levels for  $\phi=1$  are listed in Table 1. Pressure outlet boundary condition is specified at the outlet of the cylindrical combustor.

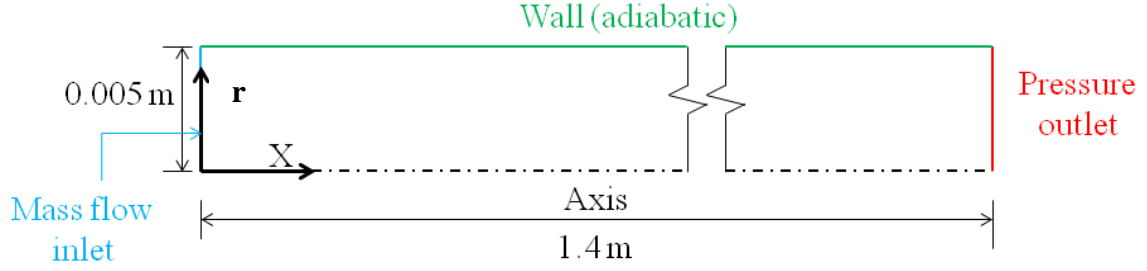


**Figure 2.** Computational domain of the combustor (not to scale)

The entire computational domain of the combustor has meshed with the help of the Ansys ICEM CFD 19.2 tool. A structured mesh with uniform size quadrilateral elements is considered, as shown in Fig.3. In axial direction (X direction), 6000 grids are considered, and in the radial direction (r direction), 40 grids are considered. This constitutes a total number of 2,40,000 grid points or 2,33,961 cells. This particular number of cells (2,33,961 cells) has been chosen in our present work after conducting a grid independence test. The temperature variations along the centerline of the tubular combustor for 1300 K reactant temperature and 21 %  $O_2$  and operating at 1atm pressure are chosen for the grid independence. The grid independence test is shown in Fig.S1 of the supplementary material.

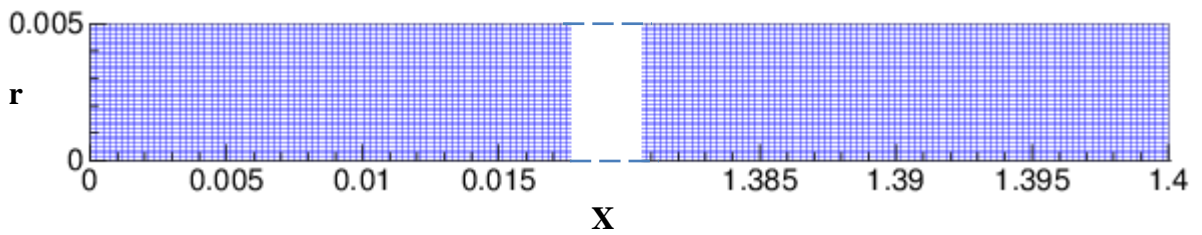


**Figure 3.** The meshing of the computational domain

The laminar premixed  $CH_4/O_2/N_2$  flames are computed by a set of conservation equations for continuity, momentum, energy, and species in a 2-D axisymmetric computational domain using finite-volume-based commercial CFD code Ansys Fluent 19.2. The steady-state assumption is

adopted in the current computation. Volumetric reaction-based finite rate chemistry with the detailed chemical mechanism GRI Mech 3.0 (Smith et al., 2019) is used for the combustion analysis. Many researchers have considered GRI Mech 3.0 chemical mechanism for their CFD investigations at atmospheric and elevated pressure (Kruse et al., 2015; Mardani et al., 2019; Tu et al., 2020). The chemical source term in the reactive flow is determined by the direct integration method. The discrete ordinate (DO) model with the weighted sum of the grey gas model (WSGGM) recommended by Smith et al. (1982) is considered to calculate the radiative heat transfer by correctly predicting emission and absorption co-efficient. Incompressible ideal gas law is used to calculate the density of all the species. The SIMPLE algorithm is used for pressure-velocity coupling to solve the pressure correction equation. The second-order upwind scheme is used to discretize the convective part of the transport equation for more accurate calculations. A central difference scheme is utilized to discretize the diffusive component of the governing equations. The convergence criteria for each simulation are set through two critical conditions. First, the residuals for all the equation is set below  $10^{-6}$ , except for energy and radiation equation with a stricter tolerance of  $10^{-8}$ . Second, the variation of velocity and mean temperature at the combustor outlet are less than 0.1m/s and 1 K, respectively.

## **2.4. Validation of CFD work**

The validation of the present numerical methodology is checked by comparing the profiles of flame temperature and species concentration with the experimental data available in the literature. It is not possible to compare the result of the present numerical work with the experiments performed in such size geometry at atmospheric and elevated pressure since there are non-available. However, some experimental data were found for a one-dimensional flame geometry with a stoichiometric methane-air mixture conducted in the atmosphere (Bechtel et al.,

1981; Stephenson, 1979). Bechtel et al. (1981) used the Laser Raman Scattering method in their experiment to measure profiles of temperature and species concentration of stoichiometric, premixed laminar methane-air flames. The burner details can be found in the work of (Bechtel, 1979; Bechtel et al., 1981; Stephenson, 1979).

The centerline variation of profiles of temperature and species concentration by the present CFD work compared with that of experimental data from the literature Bechtel et al. (1981), as shown in Fig. S2(a)-(d) in the supplementary material. The reactant temperature and velocity for the stoichiometric methane-air mixture at the inlet are considered as 300 K and 0.3 m/s, respectively. The result shows reasonable agreement between the present numerical method with experimental data. Hence, the adopted numerical methodology is suitable for capturing the combustion behavior for the cases considered in the current work.

### **3. RESULT AND DISCUSSION**

#### **3.1. Ignition delay time**

Numerical simulation is conducted to evaluate the effect of operating pressure, reactant temperature, and dilution on ignition delay times of stoichiometric  $\text{CH}_4/\text{O}_2/\text{N}_2$  mixtures. The analysis has been carried out in the pressure range of 1-10 atm, a temperature range of 1100-1500 K, and with a range of dilution, which is carried out in terms of varying  $\text{O}_2$  content in the mixture, i.e., from 21-3%  $\text{O}_2$  (mole basis). The results are presented in Fig.4. It may be noticed from the figure that the ignition delay times of the  $\text{CH}_4/\text{O}_2/\text{N}_2$  mixtures decrease sharply at higher reactant temperatures while operating at a fixed pressure. The ignition delay for  $\text{CH}_4/\text{O}_2/\text{N}_2$  mixtures with 21%  $\text{O}_2$  and at 1 atm pressure is observed to be  $2.06 \times 10^5 \mu\text{s}$  at 1100 K, which drops down to  $1.18 \times 10^3 \mu\text{s}$  at 1500 K. Similarly, with 3%  $\text{O}_2$  level, the ignition delay is reduced from  $2.04 \times 10^6$

to  $7.49 \times 10^3 \mu\text{s}$  with increasing the reactant temperature from 1100 to 1500 K, respectively, as shown in Fig. 4(a). The dilution effect on ignition delay time can also be understood both from Fig.4 and Fig.5. The ignition delay time increases with the decrease in  $\text{O}_2$  content for a fixed inlet temperature and pressure. The variation of ignition delay time with different  $\text{O}_2$  content as a function of reactant temperature at 1 and 10 atm pressure is shown in Fig.5. For a reactant temperature of 1100 K and at 1 atm pressure, the ignition delay offers a value of  $2.06 \times 10^5$  and  $2.04 \times 10^6 \mu\text{s}$  for 21 and 3%  $\text{O}_2$  levels, respectively. Whereas for 10 atm, the ignition delay time is increased from  $1.73 \times 10^4$  to  $1.42 \times 10^5 \mu\text{s}$  with decreasing the  $\text{O}_2$  level from 21 to 3%. Likewise, for the reactant temperature of 1500 K and 1 atm pressure, the ignition delay times of  $1.87 \times 10^2 \mu\text{s}$  and  $1.66 \times 10^3 \mu\text{s}$  are observed for 21 and 3%  $\text{O}_2$ , respectively. At higher pressure of 10 atm, the ignition delay times are 6.31 and 4.51 times lower as compared to ignition delay times of 1 atm pressure for 21 and 3%  $\text{O}_2$ , respectively, while at a fixed reactant temperature of 1500 K. Next is the variation of ignition delay, which shows a non-uniform increment with the decrease of oxygen content. The increment of ignition delay is observed lower at high oxygen content and higher at low  $\text{O}_2$  content. From Fig.4(a), it can be noticed that the ignition delay time is increased by  $3.20 \times 10^3 \mu\text{s}$  and  $5.16 \times 10^4 \mu\text{s}$  on decreasing the  $\text{O}_2$  content from 21 to 17% and 5 to 3% respectively, for a fixed pressure of 1 atm. Similarly, at 10 atm pressure, the ignition delay time is increased by  $4.10 \times 10^2 \mu\text{s}$  and  $6.94 \times 10^3 \mu\text{s}$  for the decrease of  $\text{O}_2$  content from 21 to 17% and 5 to 3%, respectively, as observed from Fig.4 (e).

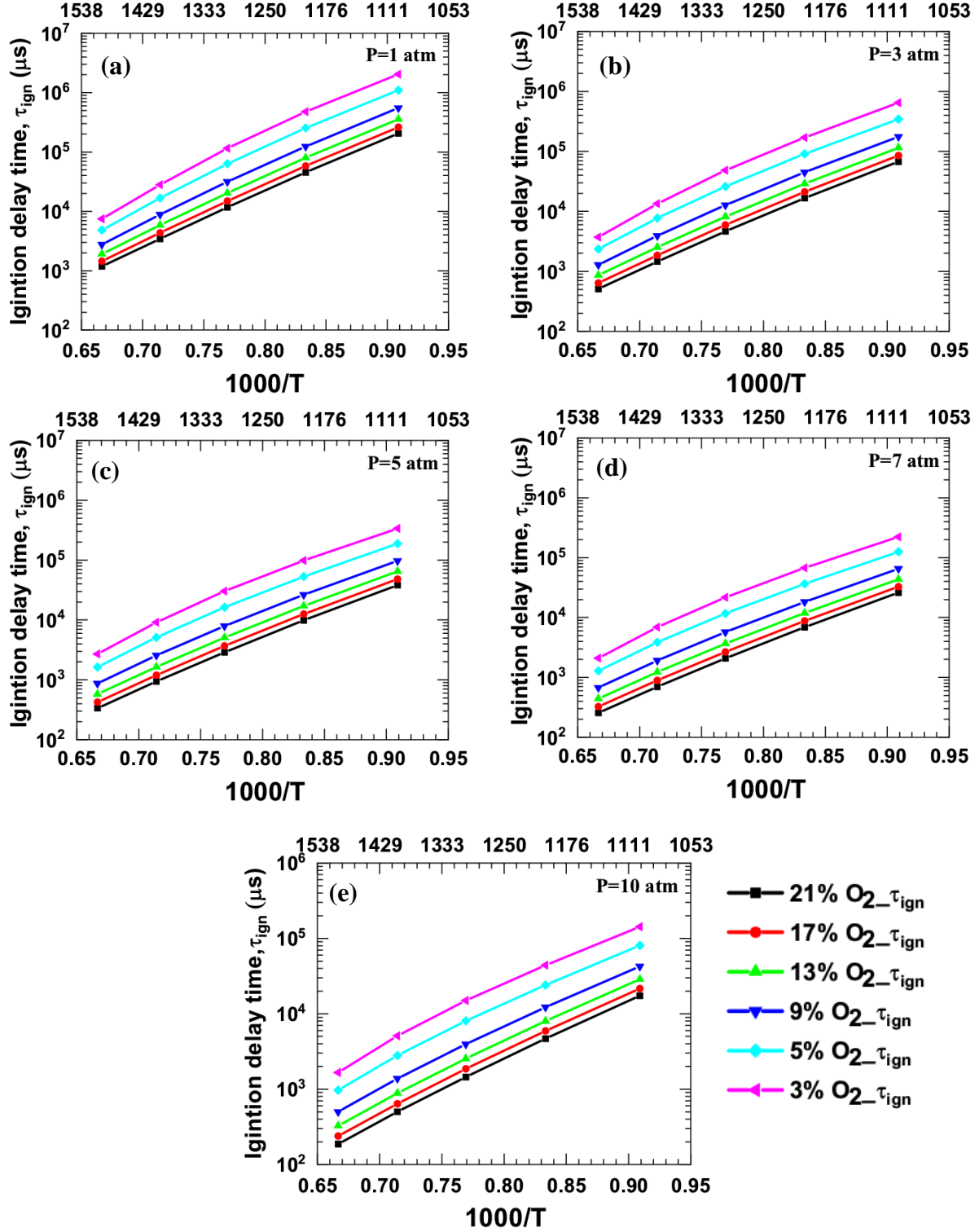


**Figure 4.** Variation of  $\tau_{ign}$  concerning different reactant temperatures of reactants at  $\phi=1$  (a) 1 atm, (b) 3 atm, (c) 5 atm, (d) 7 atm and (e) 10 atm.



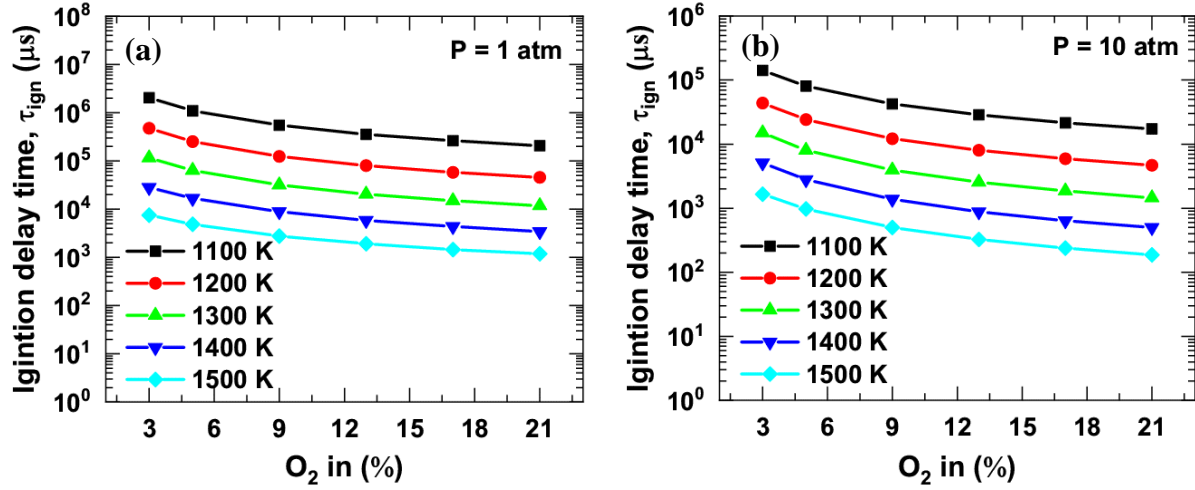


**Figure 5.** Variation of  $\tau_{ign}$  with different O<sub>2</sub> content as a function of reactant temperature for  $\phi=1$ ; (a) 1 atm and (b) 10 atm.

The effects of operating pressure on the mixture ignition delay times for 21 and 3% O<sub>2</sub> cases are shown in Fig. 6. It is observed that the ignition delay time is in inverse relation with both combustor pressure and reactant temperature. The ignition delay times get shorter with increasing the operating pressure as well as the reactant temperature. For the 21% O<sub>2</sub> level, the ignition delay time is decreased from  $1.17 \times 10^4$  to  $1.45 \times 10^3 \mu s$  as the pressure of the reactor is increased from 1 to 10 atm. While, for 3% O<sub>2</sub> content, the ignition delay times of  $1.15 \times 10^5 \mu s$  and  $1.5 \times 10^4 \mu s$  are observed for the case of 1 and 10 atm, respectively, while maintaining a fixed reactant temperature of 1300 K.

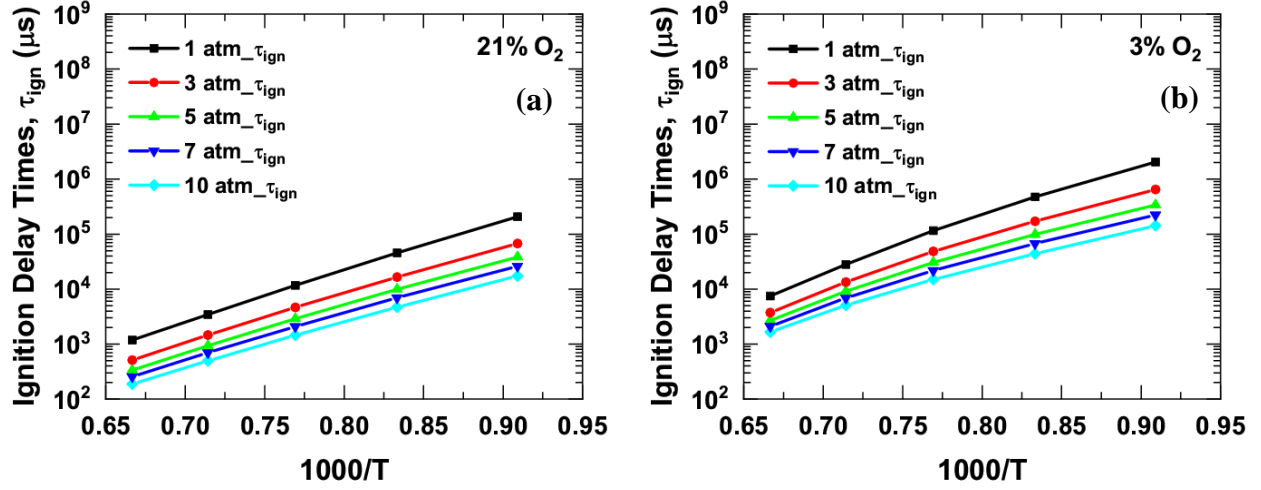


**Figure 6.** Variation of  $\tau_{ign}$  with reactant temperature at different operating pressures; (a) 21%  $O_2$ , and (b) 3%  $O_2$  levels.

### 3.2. 1-D PFR and 2-D CFD analysis

#### 3.2.1. Effect of dilution on combustion and emission characteristics.

The temperature profile of the diluted laminar premixed flame obtained by PFR data with  $O_2\%$  ranging from 21 to 3% for 1 and 10 atm pressures is shown in Fig. 7. The temperature of the reactants is kept at 1300 K for both cases. It is observed that with the decrease in oxygen level, the flame stabilizes far away from the inlet since the  $\tau_{ign}$  of the mixture ( $CH_4 + \text{oxidizer}$ ) is increased with an increase in dilution levels (Refer to Fig.4 and Fig. 5). For example, the ignition delay time of  $1.17 \times 10^4 \mu s$  and  $1.15 \times 10^5 \mu s$  is observed for the mixtures with 21 and 3%  $O_2$  levels, respectively, at 1 atm pressure. A reduction of  $O_2$  content in the mixture simultaneously decreases both  $CH_4$  and  $O_2$  content at the inlet to maintain the constant equivalence ratio ( $\phi = 1.0$ ) for all cases (refer to Table 2). The peak temperature is reduced with the decrease in oxygen content in the oxidizer. The peak temperature is observed higher for 21%  $O_2$  content and lower for 3%  $O_2$  content. However, the flame is not observed at 3 and 5%  $O_2$  content when the combustor is

operating at 1 atm pressure. Due to the higher ignition delay time ( $1.15 \times 10^5 \mu\text{s}$ ) of the mixture at 3%  $\text{O}_2$ , which is 9.83 times higher than the 21%  $\text{O}_2$  case of the same pressure. The length of the combustor is fixed to 1.4 m that is not sufficient to stabilize the flame before the exit. However, for 10 atm pressure with 3%  $\text{O}_2$ , the flame is stabilized in the combustor. The  $\tau_{ign}$  for this case is  $1.5 \times 10^4 \mu\text{s}$ , and it is 7.67 times less than the  $\tau_{ign}$  of 1 atm with 3%  $\text{O}_2$  level. Hence the flame is stabilized inside the combustor for 3%  $\text{O}_2$ , as shown in Fig. 7(b).

Furthermore, higher temperature increment is observed at high pressure. For instance, the temperature increment of 1511 K is observed at 10 atm pressure with 21%  $\text{O}_2$ ; it is 143 K more than its respective counterparts at 1 atm, as listed in Table 2. As it moves towards low  $\text{O}_2$  content, the difference in temperature decreases between 1 and 10 atm, i.e. at low  $\text{O}_2$  content, the difference of peak temperature between 10 and 1 atm is having a lower value than at high  $\text{O}_2$  content (refer Table 3). The 2-D pictorial representation of the same is shown in Fig.8. The distance of the flame front from the combustor inlet is found longer in the case of 1 atm than 10 atm, for the same dilution level, see Fig. 8(a) and (b). Also, the distance of the flame front from the combustor inlet increases with the decrease in oxygen content from 21 to 3%, which is better observed at 1 atm. At 10 atm pressure, the flame is observed very close to the inlet of the combustor due to the low  $\tau_{ign}$  of the mixture at 10 atm compared to 1 atm. Ignition delay of the mixture consisting of 21 %  $\text{O}_2$  at 10 and 1 atm pressures are  $1.45 \times 10^3 \mu\text{s}$  and  $1.17 \times 10^4 \mu\text{s}$ , respectively. The shorter ignition delay time at high pressure is responsible for the early initiation of the reaction. The dilution level ( $\text{O}_2$ ) has shown much influence on the flame stabilization location at low pressure. Flame location is justified where the sharp temperature rise is observed, as shown in Fig. 7 for all the cases. For the 1 atm pressure case, the flame front is moved from 0.35 to 0.94 m when the  $\text{O}_2$  is varied from 21 to 9 %. For 10 atm pressure, the flame front is located at 0.0055 m for 21%  $\text{O}_2$  and 0.044 m for

3% O<sub>2</sub> level. The corresponding flame location can also be observed from the temperature contour obtained from the CFD simulation. The data obtained by CFD is slightly underpredicting compared to PFR data in terms of the flame front location. Comparing CFD and PFR for the axial variation of temperature is observed from Fig. S3 of the supplementary material.

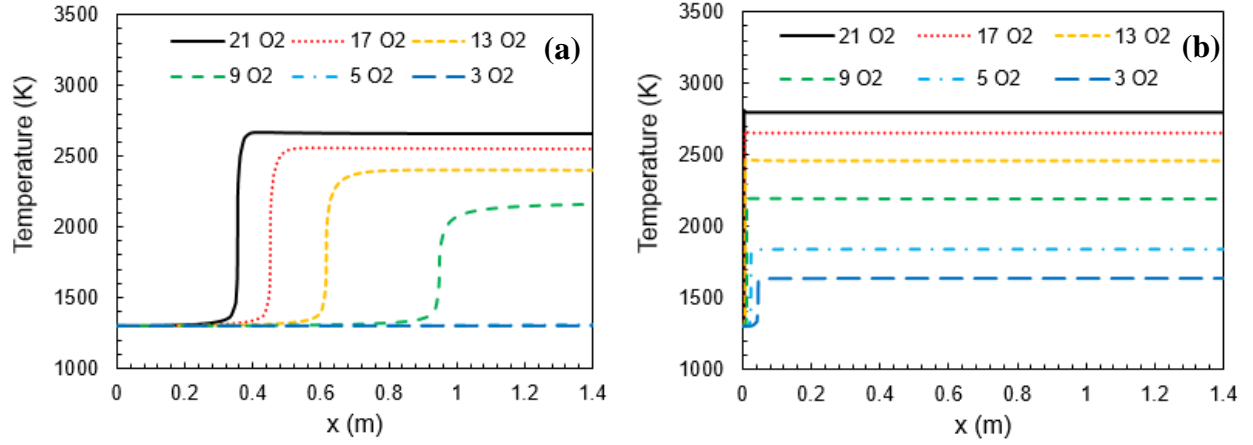


**Figure 7.** The laminar's temperature profile diluted premixed flames along the axial direction obtained from the PFR model for a reactant temperature of 1300 K; (a) 1 atm and (b) 10 atm.

**Table 2.** Temperature increment as a function of O<sub>2</sub> content at 1 and 10 atm

Pressure	$\Delta T = (T_{Peak} - T_{in})$					
	21 % O <sub>2</sub>	17 % O <sub>2</sub>	13 % O <sub>2</sub>	9 % O <sub>2</sub>	5 % O <sub>2</sub>	3% O <sub>2</sub>
1 atm	1368 K	1260 K	1103 K	860 K		
10 atm	1511 K	1365 K	1167 K	894 K	540 K	335 K

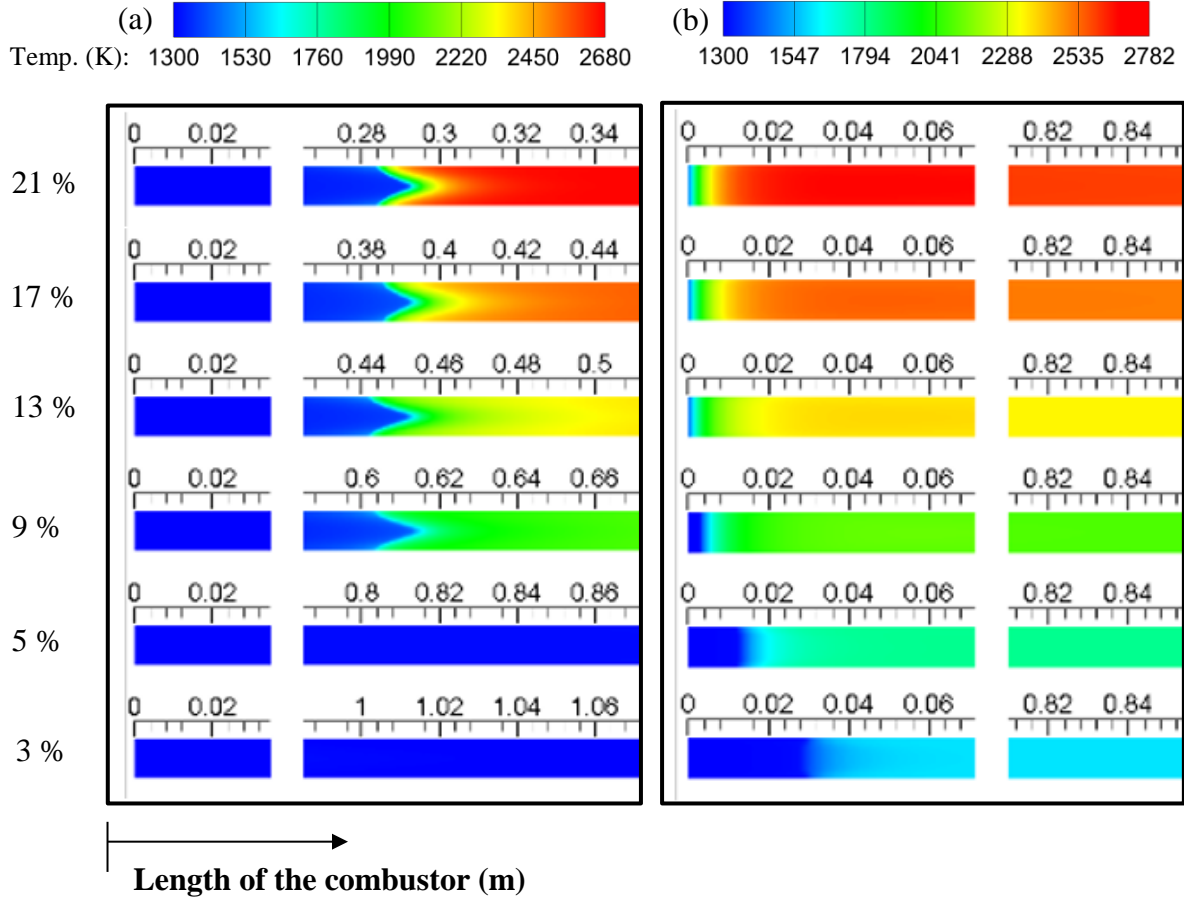
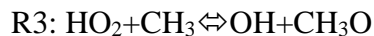
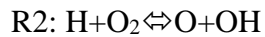
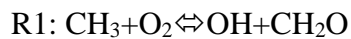


**Figure 8.** Effect of dilution level (% O<sub>2</sub> content) on temperature contour at 1300 K; (a) 1 atm and (b) 10 atm pressures.

Moreover, the flame marching is not uniform with the change in O<sub>2</sub> content, as shown in Fig. 7 for both the pressure of 1 and 10 atm. Here, the flame marching is defined as the distance between the two points of maximum slope (temperature gradient,  $\frac{dT}{dx} = \text{maximum}$ ) on the temperature variation curve for the two successive O<sub>2</sub> content. The flame marching of 0.084 m, 0.168 m, and 0.336 m is observed at 1 atm pressure for the successive decrease of O<sub>2</sub> content from 21 to 17%, 17 to 13%, and 13 to 9%, respectively. Similarly, the flame marching distance of 0.0012 m, 0.002 m, 0.0042 m, 0.0122 m, and 0.0207 m is observed for the successive decrease of O<sub>2</sub> content from 21 to 17%, 17 to 13%, 13 to 9%, 9 to 5% and 5 to 3%, respectively for 10 atm case. It indicates an increase of

flame marching distance concerning the decrease of O<sub>2</sub> content. Also, the flame marching distance is observed more for a combustor operating at low pressure than the high-pressure combustor. This non-uniform marching distance with the change of O<sub>2</sub> content is related to the variation of ignition delay time to the O<sub>2</sub> content, as shown in Fig. 4(e). The ignition delay time difference of  $4.10 \times 10^2 \mu\text{s}$ ,  $6.90 \times 10^2 \mu\text{s}$ ,  $1.40 \times 10^3 \mu\text{s}$ ,  $4.11 \times 10^3 \mu\text{s}$ , and  $6.94 \times 10^3 \mu\text{s}$  is observed for the successive decrease of O<sub>2</sub> content from 21 to 17%, 17 to 13%, 13 to 9%, 9 to 5% and 5 to 3%, respectively when the reactor is operated at 10 atm. Furthermore, an increase of ignition delay times with pressure shows a non-uniform trend, reflected upon the flame marching behavior, as shown in Fig. 7(b).

Intermediate species profiles, specifically OH, CH<sub>2</sub>O, and HCO varying with dilution level for the operating pressure of 1 and 10 atm, are shown in Fig.9. The species, such as OH and CH<sub>2</sub>O, show a wider and shorter peak at low O<sub>2</sub> content. The presence of OH in the reactive system is an indicator of reaction rate or a marker of flame, while the species, such as CH<sub>2</sub>O and HCO is an indicator of ignition and heat release rate, respectively (Mardani and Mahalegi, 2019). Figure 9(a) and (b) shows the  $X_{OH}$  profile obtained by PFR data for two operating pressures of 1 and 10 atm for the reactant temperature of 1300 K when O<sub>2</sub> is varied from 21 to 3%. It is noticed that with the decrease in O<sub>2</sub> content, the mole fraction of OH gets decreased. The reduced O<sub>2</sub> content in the mixture increases the ignition delay that helps in distributing the reaction in the combustor by minimizing the localized reaction. Reduced O<sub>2</sub> and subsequent CH<sub>4</sub> in the reactants suppress the production of OH, mainly through these reactions (Zeng et al., 2015).



It is observed from the reaction sensitivity analysis of Zeng et al. (2015)  $\text{CH}_3$  radicals formed by the dissociation of  $\text{CH}_4$  get decreased as  $\text{CH}_4$ , and  $\text{O}_2$  concentrations are reduced with increased  $\text{N}_2$  dilution. Hence, the production of OH is suppressed by the combined effect of reduced  $\text{CH}_3$  and  $\text{O}_2$ . From Fig. 9 (a), it is observed that the peak value of  $X_{\text{OH}}$  is found highest at 21%  $\text{O}_2$  and lowest at 9%  $\text{O}_2$  when the combustor is operated at 1 atm. Hence the reaction is distributed at high dilution. The species  $\text{CH}_2\text{O}$  is proven to be the precursor of auto ignition and typically appears before the ignition process. The  $\text{CH}_2\text{O}$  mole fraction is decreased as we move towards reducing the oxygen content from 21 to 3%, as shown in Fig.9 (c) and (d). By lowering the  $\text{O}_2$  content, it can be noticed that the maximum value of the mole fraction of HCO is decreased for both 1 and 10 atm, as shown in Fig.9 (e)-(f). It indicates a reduction in heat release rate at a high dilution level. The peak value of the OH and HCO mole fraction is noticed higher at 1 atm than at 10 atm while maintaining the fixed  $\text{O}_2$  content. However, the opposite is true for the  $\text{CH}_2\text{O}$  mole fraction. The maximum value of  $\text{CH}_2\text{O}$  mole fraction is observed slightly higher in the case of 10 atm than 1 atm. The profiles of the OH,  $\text{CH}_2\text{O}$ , and HCO mole fractions at a high dilution level of 3 and 5%  $\text{O}_2$  content are not observed in 1 atm while observed at 10 atm due to higher ignition delay times at 1 atm as compared to 10 atm.

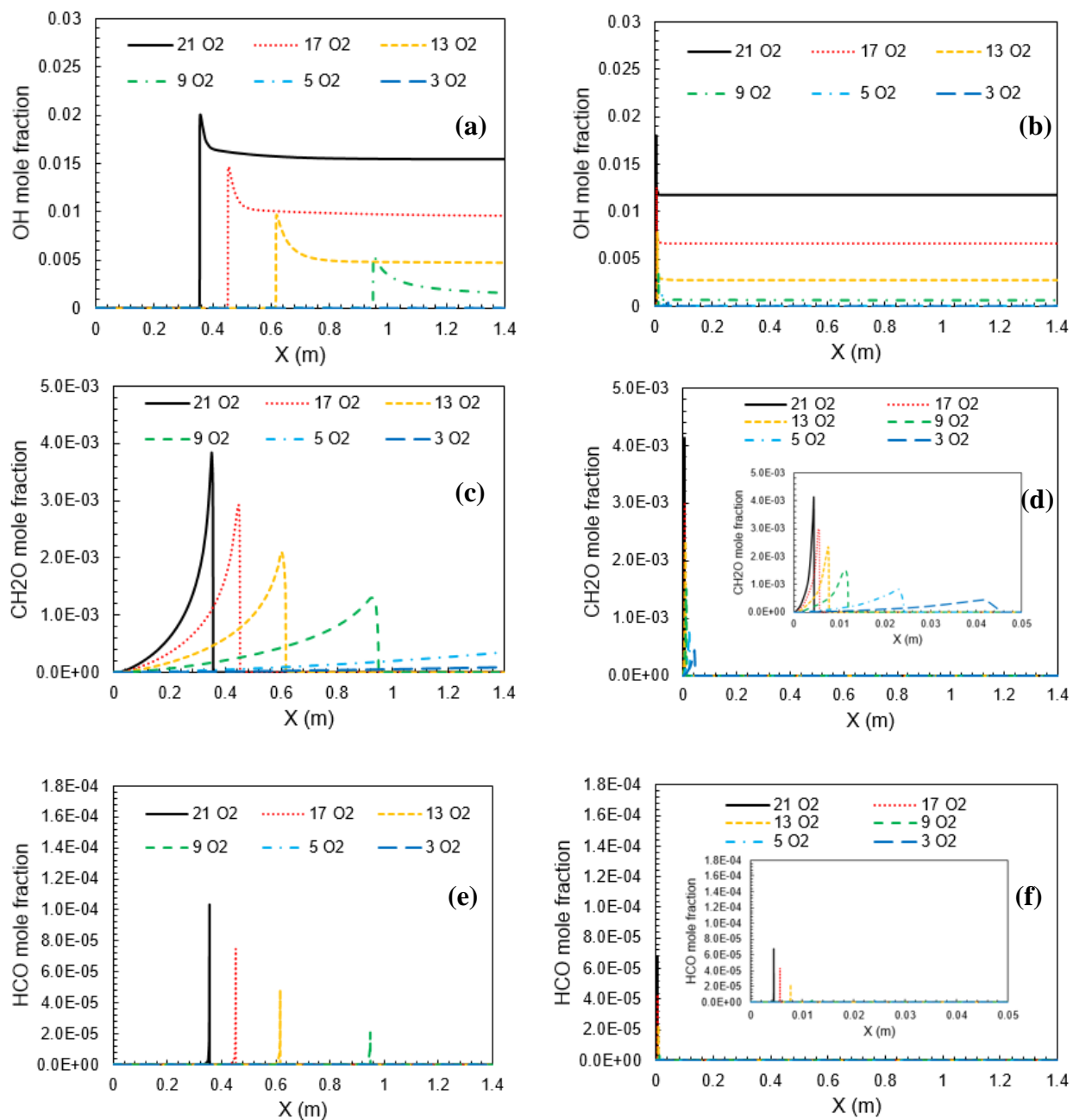


**Figure 9.** The profiles of mole fraction of the OH, CH<sub>2</sub>O, and HCO varying with dilution level along the axial direction obtained by the PFR model for the reactant temperature of 1300 K; (a),(c),(e) 1 atm, and (b),(d),(f) 10 atm.



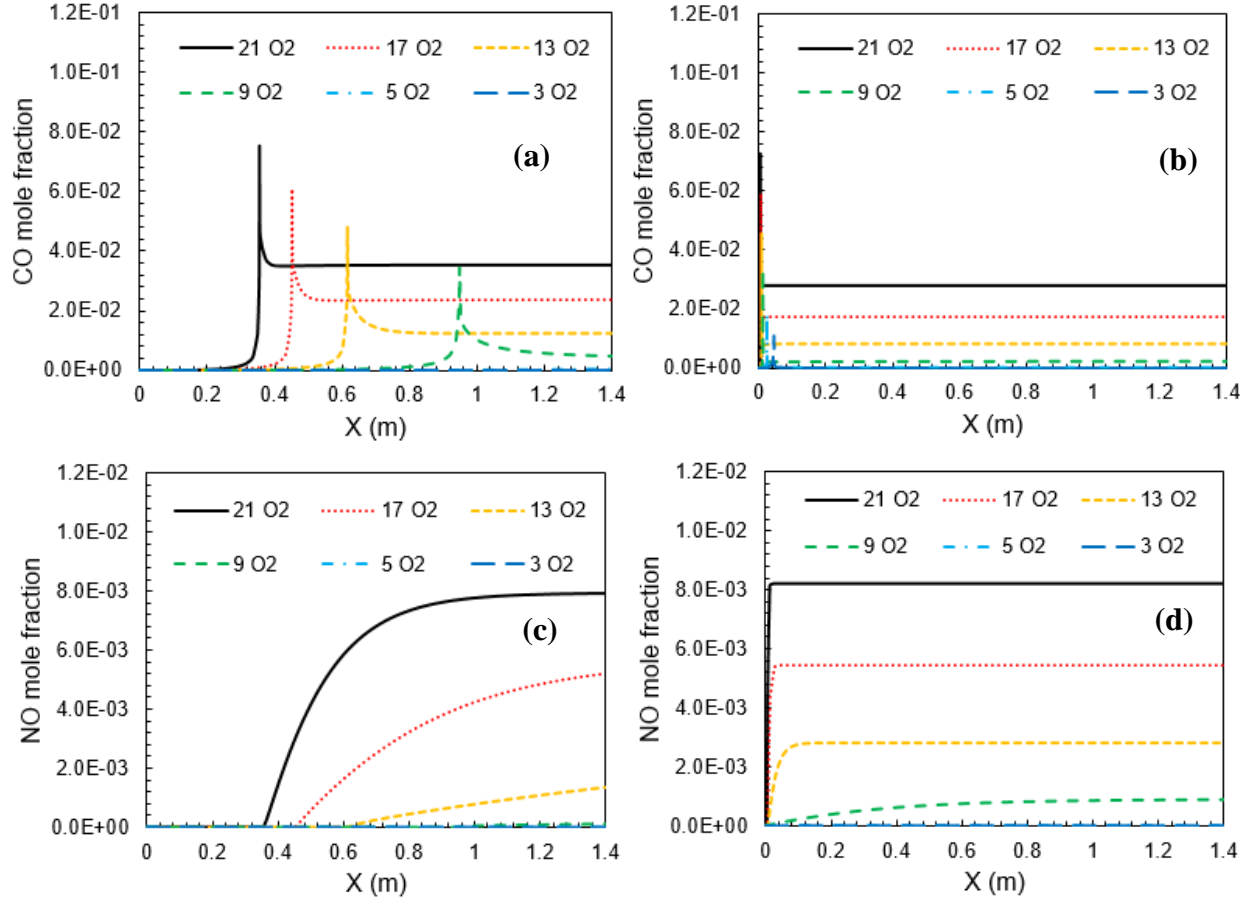


**Figure 10.** The profiles of CO and NO emission along the axial direction of the combustor; (a),(c) 1 atm, and (b),(d)10 atm.

Figure 10(a)-(d) shows the profiles of CO and NO mole fraction with  $O_2\%$  varying from 21 to 3% in the oxidizer at 1 and 10 atm, respectively. The CO mole fraction is decreased with the reduction in  $O_2$  content in the oxidizer. It can also be observed from the CO profiles that the CO mole fraction first attains a peak and then reaches the equilibrium value. Both the peak value of CO mole fraction and the CO mole fraction at the exit is decreased with the reduction in  $O_2$  content. Similarly, the NO mole fraction is reduced with the decrease in  $O_2$  content in the oxidizer. It is expected since the peak temperature is reduced at a high dilution level.

### 3.2.2. *Effect of pressure on combustion and emission characteristics*

The effect of the operating pressure on the profiles of flame temperature obtained from PFR data is shown in Fig. 11 (a) and (b). If attention is given to first Fig.11 (a), it is observed that at a high dilution level of 3% O<sub>2</sub>, the flame is not observed at 1 and 3 atm pressure while the well-stabilized flame is noticed at a higher pressure of 5,7 and 10 atm pressure. In the cases where the flame is not stabilized in the combustor, ignition delay times of these mixtures are observed very high such that the residence time of the reactants in the tube length (1.4 m) is less than the ignition delay time. As demonstrated by Burke et al.(2015), with the help of sensitivity analysis, the pressure increment inside the combustor causes an increase in concentration (high density) of reactants (CH<sub>4</sub> and oxidizer) which results  $\tau_{ign}$  to decrease. Extreme dilution and low reactant temperature cause an increase in the ignition delay time ( $\tau_{ign}$ ). For instance, the highest dilution (3% O<sub>2</sub>) and lowest reactant temperature of 1200 K,  $\tau_{ign}$  of  $4.76 \times 10^5$  and  $1.71 \times 10^5$   $\mu$ s are observed for 1 atm and 3 atm, respectively, see Fig.4 or Fig.5. The ignition delay is further decreased to a value of  $9.88 \times 10^4$   $\mu$ s at 5 atm pressure, results in the stable flame are observed in the combustor. The shorter ignition delay time also results in shifting the flames towards the combustor inlet. Likewise, the stable flame is observed in all the operating pressure considered in the present work when the reactant temperature is considered as 1500 K, as shown in Fig. 11 (b). It is because the ignition delay time is reduced with an increase in reactant temperature. For instance, the ignition delay of  $4.76 \times 10^5$   $\mu$ s is observed at 1200 K, which is reduced to  $7.49 \times 10^3$   $\mu$ s at 1500 K while maintaining the fixed pressure of 1 atm. It results in a stable flame at 1500 K with 1 atm pressure, while the flame is not observed at 1200 K with the same pressure.

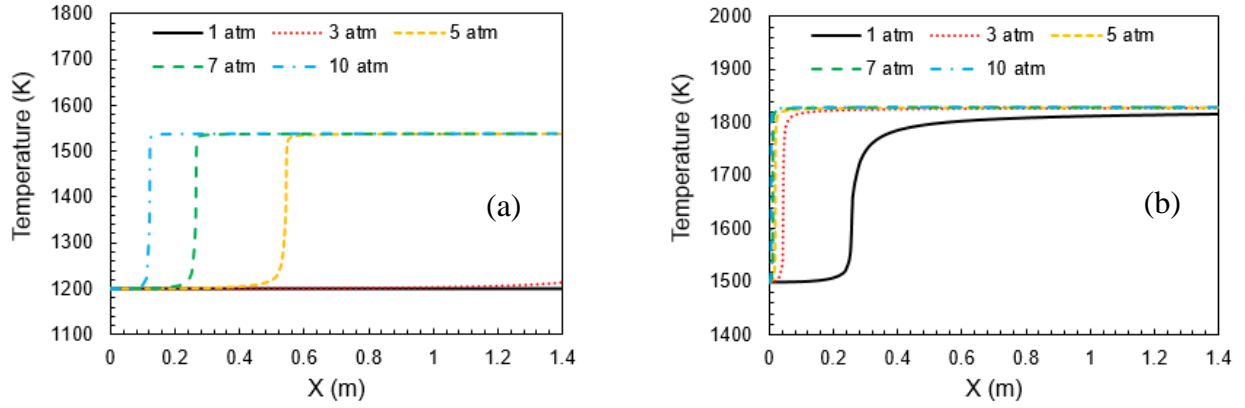


**Figure 11.** Effect of pressure on the profile of temperature obtained from PFR data for the reactant temperature of (a) 1200 K and (b) 1500 K at 3% O<sub>2</sub> level.

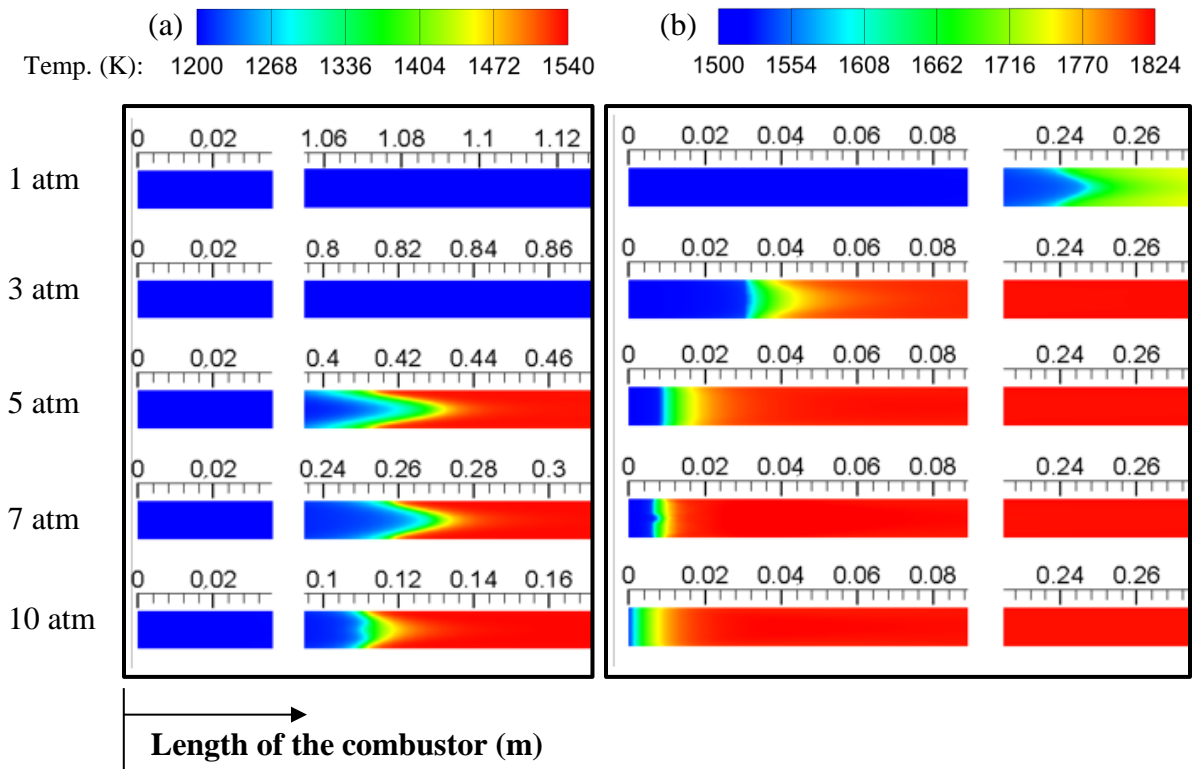


**Figure 12.** Effect of pressure on temperature contour for the reactant temperature of (a) 1200 K and (b) 1500 K at 3% O<sub>2</sub> level.

Effect of the operating pressure on flame temperature and flame marching position are shown in Fig. 11 and Fig.12 for 3% O<sub>2</sub> level at different reactant temperatures of 1200 and 1500 K. The flame front is observed closer to the combustor inlet with increasing the combustor pressure. It is due to the reduction of ignition delay times as well as jet velocity with pressure. Moreover, the flame marching is not uniform with the change in pressure, shown in Fig. 11 for both the reactant temperature. Here, the flame marching is defined as the distance between the two points of maximum slope (temperature gradient,  $\frac{dT}{dx} = \text{maximum}$ ) on the temperature variation curve for the two successive pressure. As shown in Fig. 11(b), the flame marching distance is observed more as the combustor pressure is increased from 1 to 3 atm and gradually decreased on further increasing the pressure. The flame marching distance of 0.21 m is observed when the pressure increased from 1 to 3 atm. This value is reduced to 0.025 m, 0.0073 m, and 0.00046 m on further increasing the pressure to 5, 7, and 10 atm, respectively. This non-uniform marching distance is related to the variation of an ignition delay time of the mixture with pressure. The ignition delay at 3 atm is  $3.76 \times 10^3 \mu\text{s}$  less than the pressure at 1 atm, see Fig. 4(a) and (b).

Similarly, the ignition delay time is decreased by  $1.03 \times 10^3 \mu\text{s}$ ,  $6 \times 10^2 \mu\text{s}$  and  $4.4 \times 10^2 \mu\text{s}$  on the successive increase of pressure from 3 to 5 atm, 5 to 7 atm and 7 to 10 atm, respectively, refer Fig 4(b)-(e). Furthermore, the reduction of ignition delay times with pressure shows a non-uniform trend, reflected upon the flame marching behavior, as shown in Fig. 11(b). As far as the peak temperature of the flame is concerned, the peak temperature is slightly increased from 1 to 3 atm and then after it remains almost constant with the successive increase of pressure up to 10 atm.

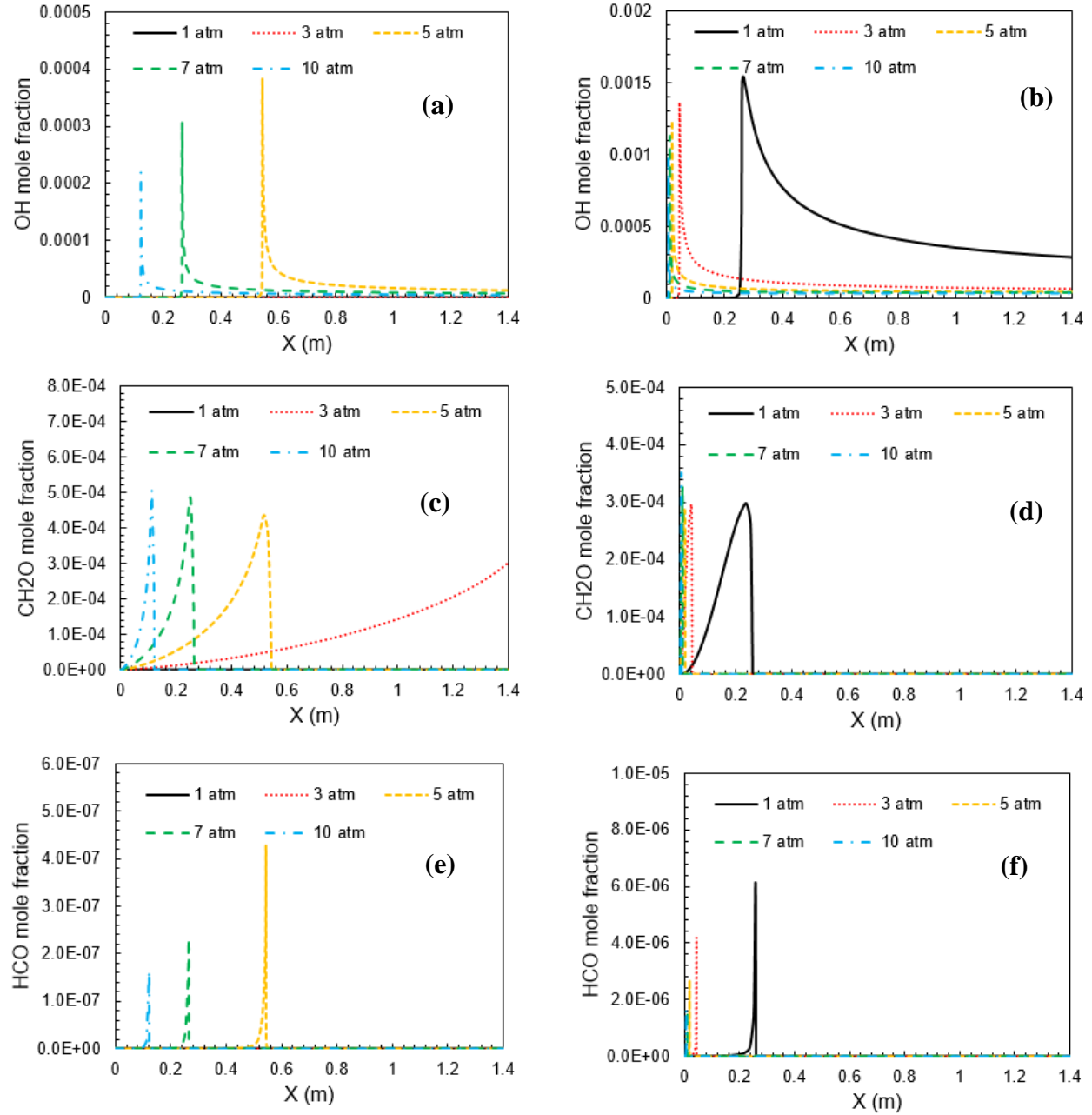


**Figure 13.** Effect of pressure on temperature contour for the reactant temperature of (a) 1200 K and (b) 1500 K at 3% O<sub>2</sub> level.

The OH mole fractions show a decreasing trend with an increase in operating pressure. It indicates a reduction in reaction rate with pressure, as shown in Fig. 13(a)-(b). Another observation is that the width of the reaction zone (the region where the OH concentration higher than 25% of

the maximum value) gets narrower with an increase in operating pressure. The peak value of the  $\text{CH}_2\text{O}$  mole fraction doesn't show a specific trend with an increase in operating pressure, as shown in Fig. 13 (c) and (d). The peak value of  $2.97 \times 10^{-4}$ ,  $2.96 \times 10^{-4}$ ,  $2.86 \times 10^{-4}$ ,  $3.24 \times 10^{-4}$ , and  $3.51 \times 10^{-4}$  are observed for the pressure of 1 atm, 3 atm, 5 atm, 7 atm, and 10 atm, respectively, while operating at fixed reactant temperature of 1500 K, as shown in Fig. 15 (d). It indicates that the peak value of  $\text{CH}_2\text{O}$  mole fraction is slightly decreased from 1 to 5 atm pressure, then after 5 atm, it starts increasing with the combustor pressure. Also, the width of the preheating zone (denoted by  $\text{CH}_2\text{O}$ ) shifts towards the combustor inlet and appears to be thinner at higher operating pressure. The  $\text{HCO}$  mole fraction is decreased with an increase in operating pressure, as shown in Fig. 10 (e) and (f). It indicates a reduction in heat release rate with operating pressure. The heat release rate is also observed lower at low reactant temperature and higher at high reactant temperature while maintaining a fixed pressure. Furthermore, the width of the heat release rate is decreased with an increase in operating pressure. The mole fraction of  $\text{OH}$  and  $\text{HCO}$  is observed lower at 1200 K reactant temperature as compared to the high reactant temperature of 1500 K. In contrast, the  $\text{CH}_2\text{O}$  mole fraction is observed higher value at 1200 K reactant temperature as compared to the reactant temperature of 1500 K. The profiles of  $\text{OH}$ ,  $\text{CH}_2\text{O}$  and  $\text{HCO}$  species at a pressure of 1 and 3 atm are not observed with the reactant temperature of 1200 K while observed with the higher reactant 1500 K due to higher ignition delay times at 1200 K as compared to 1500 K.

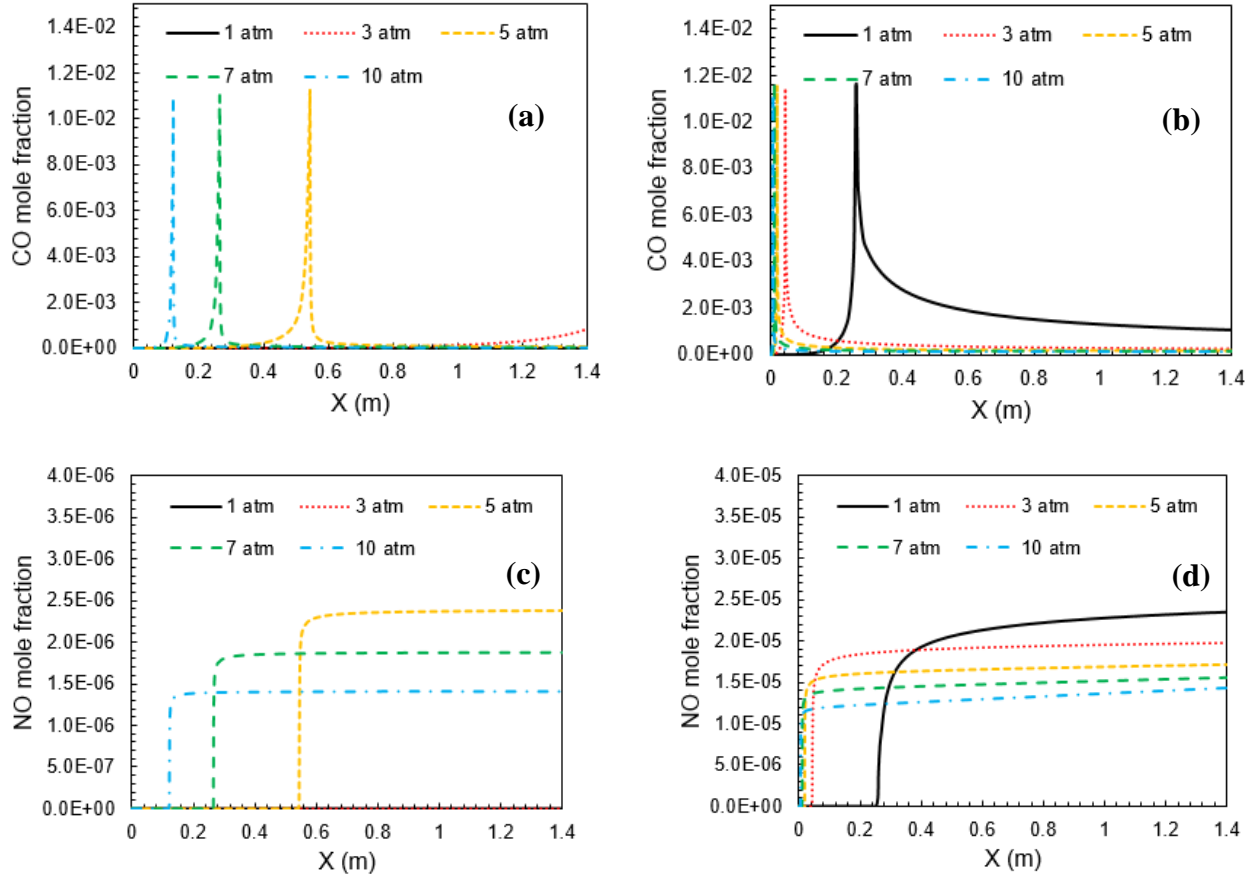


**Figure 14.** Effect of pressure on the profiles of CO and NO mole fraction at 3%  $O_2$  level; (a),(c) 1200 K, and (b),(d) 1500 K.

Figure 14(a)-(d) shows the profiles of CO and NO mole fraction varying with pressure at 3%  $O_2$  content for two reactant temperature of 1200 and 1500 K. The CO mole fraction at the combustor outlet is decreased with an increase of operating pressure, although the peak value doesn't vary much, as shown in Fig.14 (a)-(b). Similarly, an increase in pressure results in a decrease in the NO mole fraction, as shown in Fig.14 (c)-(d). The CO and NO mole fraction are having a lower value at reactant temperature of 1200 K than 1500 K. Besides, the mole fraction of CO and NO at 1 and 3 atm pressure is not observed for a reactant temperature of 1200 K while

observed for 1500 K reactant temperature due to higher ignition delay time at 1200 K as compared to 1500 K.

### 3.3. Identification of MILD combustion regime

The combustor operating under a different mode of combustion for the pressure of 1, 5, and 10 atm pressure has been represented in Fig. 17 (a)-(c) as a function of inlet reactant temperature ( $T_{in}$ ) and  $O_2$  content in the oxidizer. Three different modes of combustion have been observed; (i) HiTAC, (ii) MILD, and (iii) no-ignition. The MILD combustion regime in Fig. 17 (a)-(c) is identified with the help of conditions suggested by Cavaliere and Joannon (2004). They have defined MILD combustion as a subset of HiTAC in which the inlet reactant temperature is above the auto-ignition temperature of the combustible mixture and the temperature rise inside the combustor is lower than the mixture auto-ignition temperature. Here, the term “auto-ignition temperature” is defined as the lowest temperature below which any fuel-air mixture will not ignite in standard testing conditions at a given pressure. For methane fuel operating at atmospheric pressure, this temperature is considered 600° C or 873 K (Robinson and Smith, 1984). At elevated pressure, the auto-ignition temperature is quoted as lower than the atmospheric pressure (Caron et al., 1999; Steinle and Frank, 1995). As suggested by Caron et al. (2009), the auto-ignition temperature for methane-air mixtures with a range of pressure from 2 to 47 atm is 410° C. Steinle, and Frank (1995) have measured auto-ignition temperature for methane-air mixture with a pressure range from 50 to 1000 atm. They have observed that the auto-ignition temperature is decreased from 600°C at atmospheric pressure to 390°C at 1000 atm. Hence, in the present work, we have considered the auto-ignition temperature of 600°C (873 K) for atmospheric pressure and 410°C (683 K) for the rest of the pressures (5, 10, 15, and 20 atm). As shown in Fig. 17 (a)-(c), the regime diagram is prepared by analyzing the peak temperature of a stable temperature profile in the



combustion. For this, a wide range of numerical simulations is conducted with the help of a steady, adiabatic, one-dimensional laminar premixed plug flow reactor (PFR) model. Out of the three regions observed in Fig. 15, a region named “no-ignition” is identified in which the mixture does not get ignited. Because in this region, the residence time of the combustor is less than the ignition delay time of the mixture ( $\tau_{res} < \tau_{ign}$ ). Another small region can be thought of along the separation boundary (boundary which separates No-ignition) with a line thickness of approximately 15-20 K (in  $T_{in}$  scale) towards the 'No-ignition' region in which the reaction has not fully occurred; i.e., the reaction has just initiated at the end of the combustor with a small rise of temperature. In these cases, a fully stable temperature profile would have been observed if the length of the combustor had been more significant than the present combustor length of 1.4 m. This small region has not been shown in Fig. 15 and included in the 'No-ignition' region for the simple analysis. The 'No ignition' region is observed in a broader region in the case of 1 atm pressure, and this region gets narrower with a successive increase in pressure. This occurs due to the variation of an ignition delay time of the mixture with pressure. The ignition delay time is decreased with an increase in pressure. The ignition inside the combustor has to occur when the residence time of the mixture inside the combustor is greater than the ignition delay time of the combustor. Next, when it comes to MILD combustion region in the map at 1 atm, it is observed that the combustion system has to be operated approximately below 9%  $O_2$  and preferably above 1275 K in order to have an appearance in the MILD combustion regime. However, at a higher pressure of 5 and 10 atm, the MILD combustion region appears below approximately 6.5%  $O_2$  content in the oxidizer. It indicates that the combustion mixture needs to be highly diluted to achieve MILD combustion at high pressure compared to its respective counterparts at 1 atm. The good thing about high-pressure MILD combustion at 5 and 10 atm is that the MILD combustion

region appears in the whole range of reactant temperature considered in the present work, i.e. (1100-1500 K). However, it requires a high level of dilution as compared to 1 atm.

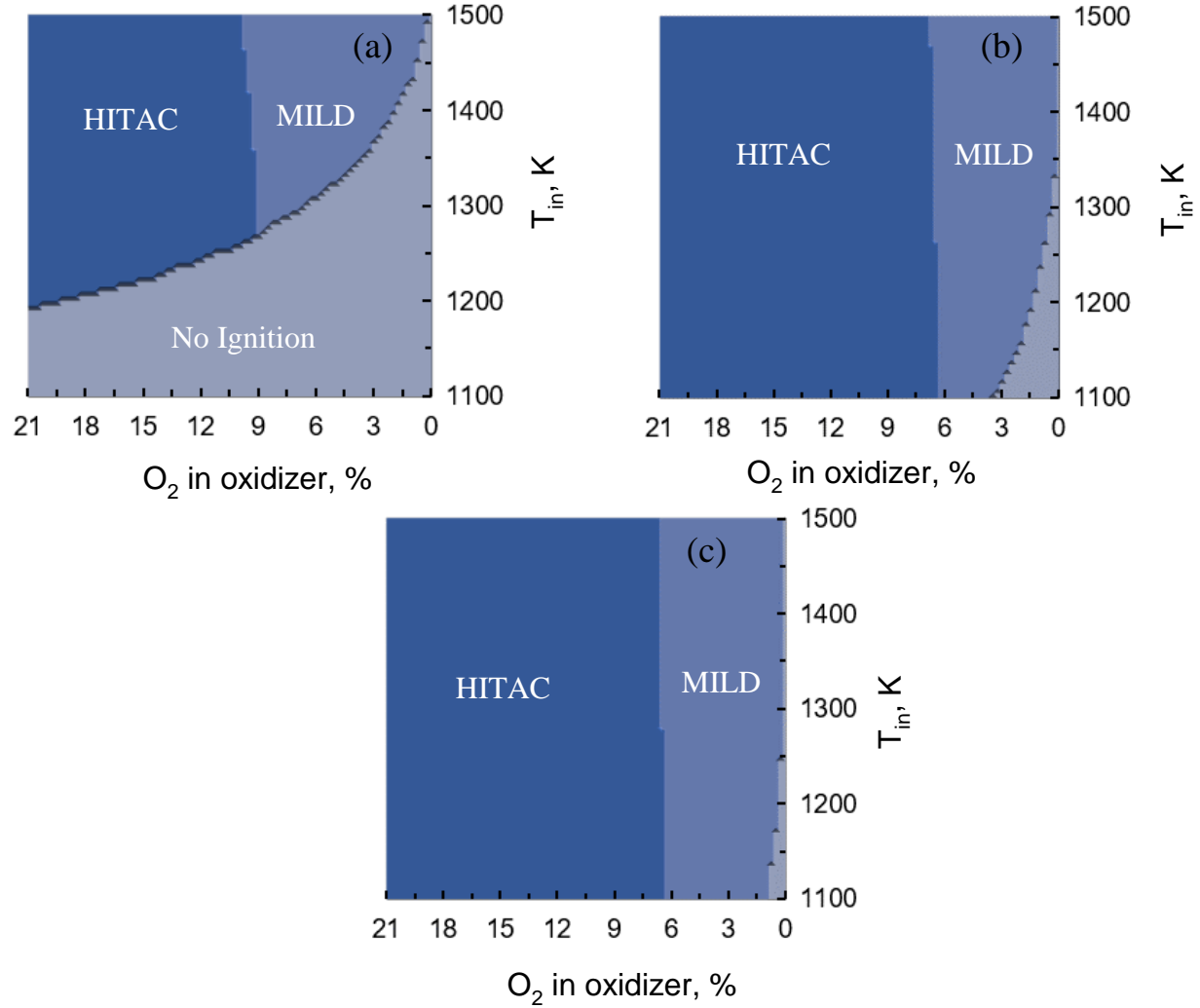


Figure 15. ( $T_{in}$ - $O_2$  in oxidizer) maps showing different modes of combustion;(a) 1 atm, (b) 5 atm, and (c) 10 atm.

Also, at a high dilution level or further reducing the  $O_2$  content in the MILD combustion regime, the reactant temperature should be increased to have a stable flame in this region. For example, if the  $O_2$  content in the mixture is decreased from 6% to 3%, the reactant temperature should be increased from 1300 K to 1350 K for 1 atm and 1100 K to 1125 K for 5 atm, respectively, to have

a stable flame in the MILD combustion regime. This can be other way stated that as we go towards the sufficiently high-level dilution or low O<sub>2</sub> content in the oxidizer to achieve MILD combustion, the reactant temperature should be increased in order to get stable flame while maintaining fixed pressure. Similarly, at a very low O<sub>2</sub> content (say 3%) in the oxidizer with a fixed low reactant temperature (say 1100 K), the pressure of the combustor needs to be increased to achieve MILD combustion. On the other hand, for a fixed reactant temperature, the combustion products need to be highly diluted to achieve MILD combustion as we go towards higher pressure.

## 5. CONCLUSIONS

High pressure laminar premixed flames in highly preheated and diluted conditions have been numerically investigated through ignition delay time, laminar PFR model, and CFD analysis. The investigations have been conducted for a wide range of operating parameters such as combustor pressure ( $1 \text{ atm} \leq P_{\text{combustor}} \leq 10 \text{ atm}$ ), reactant temperature ( $1100 \text{ K} \leq T_{\text{reactant}} \leq 1500 \text{ K}$ ), and mixture dilution ( $3\% \text{ O}_2 \leq \text{Dilution} \leq 21\% \text{ O}_2$ ). The investigation includes analyzing combustion and emission characteristics, identification of the MILD combustion regime. The significant outcomes from the present numerical studies are listed below.

- As the O<sub>2</sub> content in the mixture is decreased, the flame is stabilized at a distance far away from the combustor inlet. Similarly, with an increase in combustor pressure and reactant temperature, the distance from the combustor inlet to the flame stabilization point decreases, i.e., the flame moves towards the combustor inlet. The reason for this is summarized as varying characteristics of ignition delay times as a function of pressure, reactant temperature, and dilution. The ignition delay times are increased with the decrease in O<sub>2</sub> content, whereas it gets substantially decreased with increasing combustor pressure as well as reactant temperature.

- The residence time of the combustor increases both with increasing combustor pressure and reactant temperature. However, the peak temperature varies marginally with increasing combustor pressure while it increases with an increase in reactant temperature.
- Finally, various combustion mode such as MILD combustion, HiTAC, and No ignition is identified with the help of a regime diagram. The regime diagram is prepared as a function of reactant temperature and O<sub>2</sub> content for different operating pressure. The MILD combustion region at high pressure is observed at lower O<sub>2</sub> (below 6.5% O<sub>2</sub>) content as well as lower reactant temperature (1100 K) than the MILD combustion region at atmospheric pressure ( below 9% O<sub>2</sub> and above 1270 K). Similarly, the “No ignition” region gets decreased while the “HiTAC” region gets increased with an increase in pressure.
- Both the heat release rate and the reaction rate would appear to be low with an increase in dilution as well as pressure in the MILD combustion regime. Similarly, the width of the reaction zone as well as the heat release rate is decreased on increasing the combustor pressure.

Moreover, the CO and NO emissions observed in high-pressure MILD combustion are very low as compared to that of MILD combustion at atmospheric pressure.

### **Acknowledgment**

The present research work was carried out in the Computational Fluid Dynamics (CFD) laboratory of the Department of Mechanical Engineering at the Indian Institute of Technology, Kharagpur,

India. The research reported in this publication was partially supported by competitive research funding from King Abdullah University of Science and Technology (KAUST)".

### **References:**

- Arghode, V.K., and Gupta, A.K. 2011. Development of high intensity CDC combustor for gas turbine engines. *Appl. Energy*, **88**, 963.
- Bechtel, J.H. 1979. Temperature measurements of the hydroxyl radical and molecular nitrogen in premixed, laminar flames by laser techniques. *Appl. Opt.*, **18**, 2100.
- Bechtel, J.H., Blint, R.J., Dasch, C.J., and Weinberger, D.A. 1981. Atmospheric pressure premixed hydrocarbon-air flames: Theory and experiment. *Combust. Flame*, **42**, 197.
- Burke, U., Somers, K.P., O'Toole, P., Zinner, C.M., Marquet, N., Bourque, G., Petersen, E.L., Metcalfe, W.K., Serinyel, Z., and Curran, H.J. 2015. An ignition delay and kinetic modeling study of methane, dimethyl ether, and their mixtures at high pressures. *Combust. Flame*, **162**, 315.
- Caron, M., Goethals, M., De Smedt, G., Berghmans, J., Vliegen, S., Van't Oost, E., and vanden Aarssen, A. 1999. Pressure dependence of the auto-ignition temperature of methane/air mixtures. *J. Hazard. Mater.*, **65**, 223.
- Cavaliere, A., and de Joannon, M. 2004. Mild combustion. *Prog. Energy Combust. Sci.*, **30**, 329.
- Chen, Z., Reddy, V.M., Ruan, S., Doan, N.A.K., Roberts, W.L., and Swaminathan, N. 2017. Simulation of MILD combustion using Perfectly Stirred Reactor model. *Proc. Combust. Inst.*, **36**, 4279.
- Christo, F.C., and Dally, B.B. 2005. Modeling turbulent reacting jets issuing into a hot and diluted coflow. *Combust. Flame*, **142**, 117.

- Dally, B.B., Karpets, A.N., and Barlow, R.S. 2002. Structure of turbulent non-premixed jet flames in a diluted hot coflow. *Proc. Combust. Inst.*, **29**, 1147.
- De Joannon, M., Cavaliere, A., Donnarumma, R., and Ragucci, R. 2002. Dependence of autoignition delay on oxygen concentration in mild combustion of high molecular weight paraffin. *Proc. Combust. Inst.*, **29**, 1139.
- De Toni, A.R., Werler, M., Hartmann, R.M., Cancino, L.R., Schießl, R., Fikri, M., Schulz, C., Oliveira, A.A.M., Oliveira, E.J., and Rocha, M.I. 2017. Ignition delay times of Jet A-1 fuel: Measurements in a high-pressure shock tube and a rapid compression machine. *Proc. Combust. Inst.*, **36**, 3695.
- El Merhubi, H., Kéromnès, A., Catalano, G., Lefort, B., and Le Moyne, L. 2016. A high pressure experimental and numerical study of methane ignition. *Fuel*, **177**, 164.
- Gupta, A. 2003. High Temperature Air Combustion Technology-Invited Review. *39th AIAA/ASME/SAE/ASEE Joint Propulsion Conference and Exhibit* . 4940.
- Hu, E., Li, X., Meng, X., Chen, Y., Cheng, Y., Xie, Y., and Huang, Z. 2015. Laminar flame speeds and ignition delay times of methane–air mixtures at elevated temperatures and pressures. *Fuel*, **158**, 1.
- Katsuki, M., and Hasegawa, T. 1998. The science and technology of combustion in highly preheated air. *Proc. Combust. Inst.*, **27**, 3135.
- Khalil, A.E., and Gupta, A.K. 2011. Distributed swirl combustion for gas turbine application. *Appl. Energy*, **88**, 4898.
- Khalil, A.E., and Gupta, A.K. 2018. Fostering distributed combustion in a swirl burner using prevaporized liquid fuels. *Appl. Energy*, **211**, 513.

- Kruse, S., Kerschgens, B., Berger, L., Varea, E., and Pitsch, H. 2015. Experimental and numerical study of MILD combustion for gas turbine applications. *Appl. Energy*, **148**, 456.
- Lückcrath, R., Meier, W., and Aigner, M. 2008. FLOX® combustion at high pressure with different fuel compositions. *Journ. Eng. Gas Turbines Power*, **130**.
- Mao, Z., Zhang, L., Zhu, X., Zhou, D., Liu, W., and Zheng, C. 2017. Investigation on coal moderate or intense low-oxygen dilution combustion with high-velocity jet at pilot-scale furnace. *Appl. Therm. Eng.*, **111**, 387.
- Mardani, A., and Mahalegi, H.K.M. 2019. Hydrogen enrichment of methane and syngas for MILD combustion. *Int. Journ. Hyd. Energ.*, **44**, 9423.
- Rafidi, N., Blasiak, W., and Gupta, A.K. 2008. High-temperature air combustion phenomena and its thermodynamics. *Journ. Eng. gas turbines pow.*, **130**.
- Reddy, V.M., Biswas, P., Garg, P., and Kumar, S. 2014. Combustion characteristics of biodiesel fuel in high recirculation conditions. *Fuel process. Technol.*, **118**, 310.
- Reddy, V.M., Katoch, A., Roberts, W.L., and Kumar, S. 2015. Experimental and numerical analysis for high intensity swirl based ultra-low emission flameless combustor operating with liquid fuels. *Proc. Combust. Inst.*, **35**, 3581.
- Robinson, C., and Smith, D.B. 1984. The auto-ignition temperature of methane. *J. Hazard. Mater.*, **8**, 199.
- Sabia, P., de Joannon, M., Lavadera, M.L., Giudicianni, P., and Ragucci, R. 2014. Autoignition delay times of propane mixtures under MILD conditions at atmospheric pressure. *Combust. flame*, **161**, 3022.
- Sabia, P., de Joannon, M., Picarelli, A., and Ragucci, R. 2013. Methane auto-ignition delay times and oxidation regimes in MILD combustion at atmospheric pressure. *Combust. flame*, **160**, 47.

- Sabia, P., de Joannon, M., Sorrentino, G., Giudicianni, P., and Ragucci, R. 2015. Effects of mixture composition, dilution level and pressure on auto-ignition delay times of propane mixtures. *Chem. Eng. Journ.*, **277**, 324.
- Sabia, P., Lavadera, M.L., Giudicianni, P., Sorrentino, G., Ragucci, R., and de Joannon, M. 2015. CO<sub>2</sub> and H<sub>2</sub>O effect on propane auto-ignition delay times under mild combustion operative conditions. *Combust. flame*, **162**, 533.
- Shao, J., Choudhary, R., Davidson, D.F., Hanson, R.K., Barak, S., and Vasu, S. 2019. Ignition delay times of methane and hydrogen highly diluted in carbon dioxide at high pressures up to 300 atm. *Proc. Combust. Inst.*, **37**, 4555.
- Sidey, J., Mastorakos, E., and Gordon, R.L. 2014. Simulations of autoignition and laminar premixed flames in methane/air mixtures diluted with hot products. *Combust. Sci. Technol.*, **186**, 453.
- Smith, G.P., Golden, D.M., Frenklach, M., Moriarty, N.W., Eiteneer, B., Goldenberg, M., Bowman, C.T., Hanson, R.K., Song, S., Gardiner Jr, W.C., and Lissianski, V.V. 2020. GRI-Mech 3.0. URL: [http://www.me.berkeley.edu/gri\\_mech](http://www.me.berkeley.edu/gri_mech).
- Smith, T.F., Shen, Z.F., and Friedman, J.N. 1982. Evaluation of coefficients for the weighted sum of gray gases model. *J. Heat Transfer*, **104**, 602.
- Steinle, J.U., and Franck, E.U. 1995. High pressure combustion–Ignition temperatures to 1000 bar. *Ber. Dtsch. Bot. Ges.*, **99**, 66.
- Stephenson, D.A. 1979. Non-intrusive profiles of atmospheric premixed hydrocarbon-air flames. In *Symp. (Int.) Combust.*, **17**, 993.



- Tu, Y., Xu, S., Xu, M., Liu, H., and Yang, W. 2020. Numerical study of methane combustion under moderate or intense low-oxygen dilution regime at elevated pressure conditions up to 8 atm. *Energy*, **197**, 117158.
- Wünning, J.A., and Wünning, J.G. 1997. Flameless oxidation to reduce thermal NO-formation. *Progr. Energ. Combust. Sci.*, **23**, 81.
- Ye, J., Medwell, P.R., Varea, E., Kruse, S., Dally, B.B., and Pitsch, H.G. 2015. An experimental study on MILD combustion of prevaporised liquid fuels. *Appl. Energy*, **151**, 93.
- Zeng, W., Ma, H., Liang, Y., and Hu, E. 2015. Experimental and modeling study on effects of N<sub>2</sub> and CO<sub>2</sub> on ignition characteristics of methane/air mixture. *Journ. Adv. Research.*, **6**, 189.